

Half-metallic ferromagnetism in binary compounds of alkali metals with nitrogen: *Ab initio* calculations

Krzysztof Zborecki, Leszek Adamowicz and Michał Wierzbicki

Faculty of Physics, Warsaw University of Technology, ul. Koszykowa 75, 00-662 Warsaw, Poland

(Dated: November 2, 2018)

The first-principles full-potential linearized augmented plane-wave method based on density functional theory is used to investigate electronic structure and magnetic properties of hypothetical binary compounds of I^A subgroup elements with nitrogen (LiN, NaN, KN and RbN) in assumed three types of crystalline structure (rock salt, wurtzite and zinc-blende). We find that, due to the spin polarized p orbitals of N, all four compounds are half-metallic ferromagnets with wide energy bandgaps (up to 2.0 eV). The calculated total magnetic moment in all investigated compounds for all three types of crystal structure is exactly $2.00 \mu_B$ per formula unit. The predicted half-metallicity is robust with respect to lattice-constant contraction. In all the cases ferromagnetic phase is energetically favored with respect to the paramagnetic one. The mechanism leading to half-metallic ferromagnetism and synthesis possibilities are discussed.

PACS numbers: 71.15.Mb, 71.20.Dg, 72.25.Ba, 75.50.Cc

I. INTRODUCTION

Half-metallic (HM) ferromagnets are materials in which, due to the ferromagnetic decoupling, one of the spin subbands is metallic, whereas the Fermi level falls into a gap of the other subband. The concept of HM ferromagnet was first introduced by de Groot *et al.* in 1983 [1] on the basis of band structure calculations for NiMnSb and PtMnSb semi-Heusler alloys. HM ferromagnets are considered as promising materials to exploit the spin of charge carriers in new generations of transistors and other integrated spintronic devices [2], in particular, as a source of spin-polarized carriers injected into semiconductors, since only one spin channel is active during charge transport, thus leading to 100% spin-polarized electric current.

Since 1983 many HM ferromagnets have been theoretically predicted, but very few of them found experimental confirmation like metallic oxides CrO_2 [3] and Fe_3O_4 [4] or manganese perovskite $\text{La}_{0.7}\text{Sr}_{0.3}\text{MnO}_3$ [5]. Many HM ferromagnetic materials were predicted in transition-metals pnictides [6, 7] and chalcogenides [8, 9] by means of first-principles calculations.

Recently, an unusual class of ferromagnetic materials [10, 11, 12, 13, 14, 15], which do not contain transition-metal or rare-earth atoms, has been predicted and analysed theoretically by *ab initio* calculations. In Ref. [10] the authors present *ab initio* calculations for CaAs in zinc-blende structure, where magnetic order is created with the main contribution of the anion p electrons (“ p -electron” ferromagnetism). More comprehensive study was made in [11], where the authors investigate p -electron ferromagnetism in a number of tetrahedrally coordinated binary compounds of I/II-V elements. The characteristic feature of this class of materials is the integer value of the total magnetic moment per formula unit, which, in some combinations of elements, can be as large as $3 \mu_B$ [15]. Results presented in Ref. [12], where magnetic and

structural properties of $\text{II}^A\text{-V}$ nitrides have been investigated using *ab initio* methods, motivated us to check possibility of finding half-metallic ferromagnetism in $\text{I}^A\text{-N}$ binary compounds. Another motivation was that the atomic bonds in $\text{I}^A\text{-N}$ nitrides are supposed to be mostly ionic in nature (due to significant difference in electronegativity between I^A atoms and nitrogen atom) which was essential for appearing of p -electron ferromagnetism in all previously considered HM cases ([10]-[14]).

In this paper we present electronic structure and magnetic properties of hypothetical $\text{I}^A\text{-N}$ binary compounds (LiN, NaN, KN and RbN) with the rock salt (RS), wurtzite (WZ) and zinc-blende (ZB) crystalline structure, calculated by means of first-principles full-potential linearized augmented plane-wave method. We find that all four compounds in all three types of structures are HM ferromagnets with robust half-metallicity against lattice compression in the range from 2% for LiN (RS) up to 50% for NaN (WZ). This is crucial parameter for the practice of epitaxial growth, *e.g.* by means of MBE or MOCVD, to fabricate magnetic ultrathin layer structures for spin injection into suitable semiconductor substrate.

The paper is organized as follows. Section II shows details of our calculation method, while section III presents calculated total energy and band structure. In section IV we analyse density of states and the origin of half-metallic ferromagnetism. The paper is concluded with section V.

II. COMPUTATIONAL METHOD

All calculations were performed using WIEN2k code [16] which implements the full-potential linearized augmented plane wave (FLAPW) method [17]. Exchange and correlation were treated in the local spin density approximation (LSDA) by adding gradient terms. This GGA approximation was used in the Perdew-Burke

Ernzerhoff [18] parametrization. It should be mentioned that LSDA gives the magnetic moments in a very good agreement with experiment but underestimates the lattice constants in the case of transition metals. On the other hand, gradient corrections significantly reduce this error and give the correct phase stability but tend to overestimate the magnetic moment. We checked this deficiency of GGA in our calculations and it turned out that it has a small effect on the considered systems.

The convergence of the basis set was controlled by the cut-off parameter $RK_{\max} = 8$ together with 5000 k-point mesh for the integration over the Brillouin zone. The angular momentum expansion up to $l = 10$ and $G_{\max} = 12$ a.u.⁻¹ ($G_{\max} = 14$ a.u.⁻¹ in case of RbN) for the potential and charge density was employed in the calculations. Self-consistency was considered to be achieved when the total energy difference between succeeding iterations is less than 10^{-5} Ry per formula unit. Geometry optimization was performed allowing all atoms in the unit cell to relax, constrained to the initially assumed crystal symmetry.

III. TOTAL ENERGY AND BAND STRUCTURE

For all four compounds investigated by us the total energies E have been calculated as a function of the lattice parameter a for three crystal structures, namely RS, WZ and ZB, in ferromagnetic and paramagnetic state. We also optimized lattice constants a by minimization of the total energy E . Figure 1 presents total energy E versus lattice constant a for all three crystal structures. As one can see in all compounds the RS structure is the most energetically favored, thus, indicating the ionic bonding as prevailed coupling mechanism. Also, in all the cases, the paramagnetic phase is higher in energy than the corresponding ferromagnetic one. Calculated equilibrium lattice constants a_0 can be found in Table I as well as differences between total equilibrium energies of ferromagnetic and paramagnetic states $\Delta E_{\text{tot}}^{\text{f-p}}$.

The calculated total magnetic moment in all investigated compounds for all three types of crystal structures is exactly $2.00 \mu_B$ per formula unit. An integer value of magnetic moment is a characteristic feature of HM ferromagnetism [11]. Table I shows total values of magnetic moments for all compounds as well as contributions from I^A atoms (Li, Na, K and Rb), N atom and interstitial region to total magnetic moment. The main contribution in all cases comes from nitrogen anion ranging from $1.51 \mu_B$ for LiN in ZB to $1.85 \mu_B$ for KN in RS and ZB, which confirms the general feature that in HM ferromagnetic compounds the most of resulting global magnetic moment is carried by anion electrons. To verify that the integer value of total magnetic moment stabilizes the crystal structure, we have calculated the total energy E as a function of the total magnetic moment μ_{tot} . Indeed, Figure 2 shows that the creation of magnetic moment equal to $2.00 \mu_B$ leads to the minimization of the total

energy in all the cases.

From the application point of view it is important to study robustness of the half-metallicity with respect to lattice constant. Figure 3 shows magnetic moment as a function of lattice constant for all four compounds in three crystal structures. In the case of LiN the total magnetic moment remains integer until the lattice constant is compressed to critical value of 2.75 \AA , 3.75 \AA and 4.25 \AA for WZ, ZB and RS structures, respectively. In case of NaN, KN and RbN the values can be read from Figure 3. In all studied compounds the most promising is wurtzite structure, where half-metallicity is maintained up to contraction of the lattice parameter of 9% (LiN), 54% (NaN), 22% (KN) and 21% (RbN). Wide bandgap semiconductors AlN, GaN and ZnO in WZ crystal structure are considered as strong potential materials for spintronic applications. The spin scattering relaxation time of charge carriers during the transport process in these materials is strongly increased as compared to GaAs [19]. This means longer lifetime of electrons in particular spin state and longer spin “memory” of electrons when injected into these materials. Lattice constants of these wide bandgap semiconductors are close to 3.2 \AA , what is in the range of LiN and NaN HM ferromagnetism in WZ structure with 3% and 18% lattice mismatch, respectively. Therefore, having in mind state-of-the-art in producing artificial structures, at least some of the HM ferromagnets studied here seem to be potential candidates for epitaxial growth on AlN, GaN and ZnO substrates as layers for injection of 100 % spin polarized electrons. Most of ZB III-V semiconductors as well as narrow bandgap IV-VI semiconductors in RS structure (binary compounds of Pb with S, Se and Te) also satisfy lattice matching conditions as possible substrates for bulk growth of proposed here I^A -N compounds in HM ferromagnetic phase.

Figures 4 and 5 illustrate calculated spin resolved electron band structure for RbN at equilibrium lattice constant for three types of crystal structures. In all cases the minority spin subband is metallic, while the majority spin subbands are separated from the Fermi level by wide bandgaps of 4.22 eV, 3.48 eV and 3.45 eV in RS, WZ and ZB crystal structure, respectively. This is in contrast with the $3d$ pnictides in which the bandgap appears in the minority spin subband as a consequence of d bands splitting [7]. Three remaining compounds (LiN, NaN, and KN) also demonstrate half-metallic nature with wide bandgaps. The HM bandgaps, separating allowed energies for majority spin states from the Fermi level, are wide enough and ranging from about 0.2 eV for LiN (RS) to no less than 2.0 eV in the case of KN and RbN for three considered crystal structures. The last value is, to our knowledge, the largest one ever obtained for binary compound HM ferromagnet, thus making KN and RbN very promising materials for spintronic applications. The bands for RbN are flat and nearly dispersionless close to the Fermi level. The mechanism leading to this kind of energy bands has been discussed by other authors [11, 12]

as an important condition for stability of HM ferromagnetism.

In the case of NaN and KN the bands look very similar to those presented in Figures 4 and 5 for RbN. For LiN the situation is slightly different, because the bands near the Fermi level are more dispersive, but far from breaking down HM ferromagnetism. Table II presents calculated values of majority spin-up E_g^{up} and minority spin-down E_g^{dn} subbands main bandgaps, as well as HM bandgaps E_g^{HM} in the majority-spin subband. Decrease of main bandgaps (of direct character only in the case of RS structure) and increase of HM bandgaps with increasing atomic number of alkali metal elements is observed.

IV. DENSITY OF STATES AND HM FERROMAGNETISM

It is instructive to compare the band structure (Figs. 4 and 5) with spin resolved total and partial site and symmetry projected density of states (DOS) presented in Figure 6. There are six valence electrons in RbN (Rb: $5s^1$; N: $2s^2 2p^3$). Two of them occupy the low-energy N s states, about 11 eV below the Fermi level, and the remaining four electrons are mainly involved in filling anion N p states. The crystal field of cubic or hexagonal symmetry caused by surrounding N anions splits the Rb cation $4d$ states with three t_{2g} states (d_{xy}, d_{yz}, d_{zx}) lying lower in energy and the two e_g states ($d_{x^2-y^2}, d_{3z^2-r^2}$) lying higher. Hybridization between N p states and Rb t_{2g} or e_g $4d$ states (depending on the type of crystal lattice) creates both bonding and antibonding hybrid orbitals. The bonding orbital, lower in energy, appears at the edge of normally occupied region of N p states. The antibonding hybrid orbital remains in the Rb t_{2g} or e_g manifold but pushed up in energy relative to the non-bonding state.

The bands around Fermi level are formed mainly of N p states with small admixture of Rb d states with predominant e_g symmetry in RS structure and t_{2g} symmetry for ZB and WZ structures for both spin orientations. In contrast to the p states, the s states are placed well below or high above Fermi level giving no net spin polarization. Similarly, the bands located at higher energies (from 4.5 to 12.5 eV above the Fermi level) are mainly composed of d states belonging to t_{2g} and e_g representations. Hence, the s and d states are not directly involved in creation of spin polarisation and ferromagnetism in RbN and other I^{A} -N binary compounds.

Existence of narrow bands near Fermi level translates into peaks in the DOS diagrams. According to qualitative Stoner criterion the high density of electron states at the Fermi level should stabilize the ferromagnetic order. Pressure induced lattice contraction produces changes in the band structure, increase of band widths with increasing kinetic energy, decrease of the spin splitting and destroying ferromagnetism.

In the presented here results of the ground state total

energy calculations we can see the influence of Coulomb intra-atomic electron repulsion. It produces energy shift $\Delta = 2$ eV between narrow majority and minority spin energy band states, visible as peaks at – and below Fermi level in the DOS diagrams, shown in Figure 6. This type of band structure with well separated up and down spin states can be attributed to the Hubbard-like interaction $U = \Delta/2$. The parameter $U = 1$ eV is a measure of energy formation for magnetic moment localized at nitrogen ion. According to Hund's rule and Pauli principle the limiting value of magnetic moment for p electrons is the value of $3 \mu_B$. The four valence p electrons, present in the system, can produce magnetic moment not greater than $(3 - 1) \mu_B = 2 \mu_B$, what agrees with our calculations.

Estimation of thermodynamic stability of HM ferromagnetism requires additional calculations to determine the strength of inter-atomic exchange coupling [20]. This task requires supercell calculations for planar antiferromagnetic structure of the first (AF1) and second kind (AF2) as particular cases of spiral structure with the \mathbf{q} vector $[001]$ and $\frac{1}{2}[111]$, respectively [11]. We have performed relevant calculations only for LiN in WZ crystal structure. The energy differences are $E_{\text{AFM1}} - E_{\text{FM}} = 0.247$ eV and $E_{\text{PARA}} - E_{\text{FM}} = 0.701$ eV. The estimated lower limit for paramagnetic Curie temperature is about 464 K, what makes the material promising for experimental investigation.

V. CONCLUSIONS

On the basis of *ab initio* calculations employing density functional theory we have investigated half-metallic ferromagnetism in rock salt, wurtzite and zinc-blende compounds composed of group I^{A} alkali metals as cations and nitrogen as anion. We find that, due to the spin polarized p orbitals of N, all four compounds are half-metallic ferromagnets with wide energy bandgaps (up to 2.0 eV). The calculated total magnetic moment in all investigated compounds is exactly $2.00 \mu_B$ per formula unit. Our calculations show that the predicted half-metallicity is robust with respect to lattice constant contraction. The formation of ferromagnetic order requires large lattice constants, high ionicity, empty d orbitals and slight hybridization between N anion p states and I^{A} cation d states with energies in vicinity of the Fermi level. It is interesting to note that palladium (with its eight $4d$ electrons), as dopant replacing Ga atom in WZ GaN semiconductor, interacts with surrounding N atoms in a similar way like alkali atoms do, but hybridisation between Pd $4d$ and N p orbitals leads to formation of ferromagnetic order with Pd as the main contributor (not N) to the total magnetic moment [21].

Demonstrated here ferromagnetic order is always more energetically stable than antiferromagnetic and paramagnetic state, what makes these materials possible candidates for spin injection in spintronic devices. Calcula-

tions of the total energy indicate that this class of materials can exist in stable or metastable phase. Their highly interesting magnetic properties should encourage experimentalists to stabilize these materials in properly

coordinated structures via vacuum molecular beam epitaxy, chemical transport or laser deposition on suitable substrates.

-
- [1] R. A. de Groot, F. M. Mueller, P. G. van Engen, and K. H. J. Buschow, *Phys. Rev. Lett.* **50**, 2024 (1983).
 - [2] I. Žutić, J. Fabian, and S. Das Sarma, *Rev. Mod. Phys.* **76**, 323-410 (2004).
 - [3] S. P. Lewis, P. B. Allen, and T. Sasaki, *Phys. Rev. B* **55**, 10253 (1997).
 - [4] Yu. S. Dedkov, U. Rüdiger, and G. Güntherodt, *Phys. Rev. B* **65**, 064417 (2002).
 - [5] J.-H. Park, E. Vescovo, H.-J. Kim, C. Kwon, R. Ramesh, and T. Venkatesan, *Nature (London)* **392**, 794 (1998).
 - [6] Y.-Q. Xu, B.-G. Liu, and D.G. Pettifor, *Phys. Rev. B* **66**, 184435 (2002).
 - [7] B.-G. Liu, *Phys. Rev. B* **67**, 172411 (2003).
 - [8] W.-H. Xie, Y.-Q. Xu, B.-G. Liu, and D. G. Pettifor, *Phys. Rev. Lett.* **91**, 037204 (2003).
 - [9] I. Galanakis and P. Mavropoulos, *Phys. Rev. B* **67**, 104417 (2003).
 - [10] K. Kusakabe, M. Geshi, H. Tsukamoto, and N. Suzuki, *J. Phys.: Condens. Matter* **16** (2004) S5639.
 - [11] M. Sieberer, J. Redinger, S. Khmelevskyi and P. Mohn, *Phys. Rev. B* **73**, 024404 (2006).
 - [12] O. Volnianska, and P. Bogusławski, *Phys. Rev. B* **75**, 224418 (2007).
 - [13] G. Y. Gao, K. L. Yao, E. Şaşıoğlu, L. M. Sandratskii, Z. L. Liu and J. L. Jiang, *Phys. Rev. B* **75**, 174442 (2007).
 - [14] Chang-wen Zhang, Shi-shen Yan, and Hua Li, *phys. stat. sol. (b)* **245**, 201 (2008).
 - [15] Chang-Wen Zhang, *J. Phys. D: Appl. Phys.* **41**, 085006 (2008).
 - [16] P. Blaha, K. Schwarz, G. K. H. Madsen, D. Kvasnicka, and J. Luitz, in *WIEN2k, An Augmented Plane Wave Plus Local Orbitals Program for Calculating Crystal Properties*, edited by K. Schwarz, Techn. Universität Wien, Austria, 2001.
 - [17] E. Wimmer, H. Krakauer, M. Weinert, and A. J. Freeman, *Phys. Rev. B* **24**, 864 (1981).
 - [18] J. P. Perdew, K. Burke, and M. Ernzerhof, *Phys. Rev. Lett.* **77**, 3865 (1996).
 - [19] E. A. Barry, A. A. Kiselev, and K. W. Kim, *Appl. Phys. Lett.* **82**, 3686 (2003); L. Adamowicz, P. Borowik, A. Duduś, and M. Kiecana, *Molecular Physics Reports* **39**, 13 (2004).
 - [20] J. Kübler, A. R. Williams and C. B. Sommers, *Phys. Rev. B* **48**, 1745 (1983); J. Kübler, *J. Phys.: Condens. Matter* **18**, 9795 (2006);
 - [21] K. Osuch, E. B. Lombardi, and L. Adamowicz, *Phys. Rev. B* **71**, 165213 (2005).

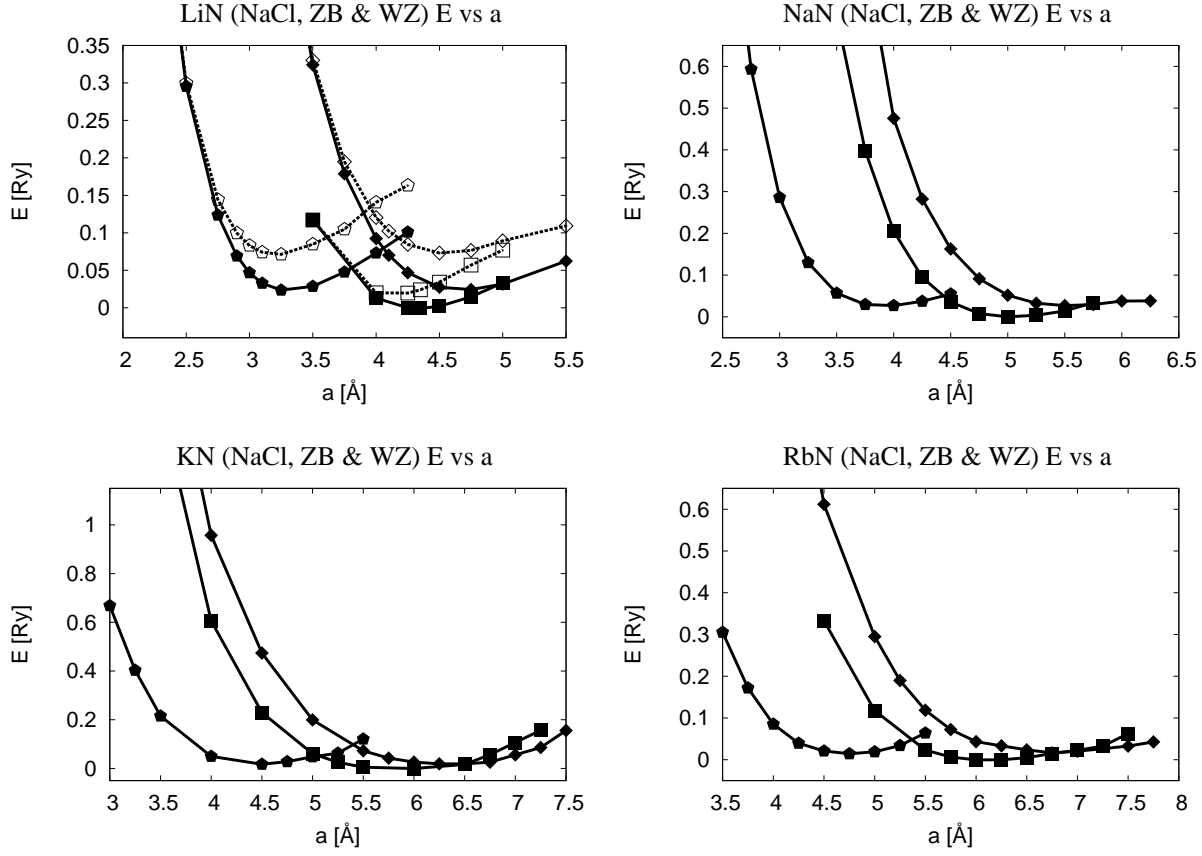


FIG. 1: Energy E (in Ry) vs. lattice constant a (in Å) for LiN, NaN, KN and RbN in three crystal structures (squares – RS, pentagons – WZ, diamonds – ZB, all for ferromagnetic phase; open symbols – the same, but for paramagnetic phase). Plots for paramagnetic energies are similar, therefore we give them only in the case of LiN.

	$a_0(\text{\AA})$	$\mu_{\text{tot}}(\mu_B)$	$\mu_{\text{IA}}(\mu_B)$	$\mu_N(\mu_B)$	$\mu_{\text{int}}(\mu_B)$	$\Delta E_{\text{tot}}^{\text{f-p}}(\text{Ry})$
LiN						
(RS)	4.36	2.00	0.06	1.72	0.21	-0.025
(WZ)	3.31	2.00	0.03	1.17	0.80	-0.102
(ZB)	4.68	2.00	0.04	1.51	0.44	-0.052
NaN						
(RS)	5.03	2.00	0.01	1.73	0.26	-0.061
(WZ)	3.91	2.00	0.02	1.47	0.51	-0.141
(ZB)	5.49	2.00	0.01	1.67	0.31	-0.074
KN						
(RS)	5.82	2.00	0.02	1.85	0.12	-0.075
(WZ)	4.51	2.00	0.03	1.75	0.22	-0.160
(ZB)	6.38	2.00	0.03	1.85	0.11	-0.080
RbN						
(RS)	6.12	2.00	0.03	1.83	0.13	-0.074
(WZ)	4.75	2.00	0.03	1.73	0.24	-0.156
(ZB)	6.70	2.00	0.03	1.83	0.13	-0.077

TABLE I: Equilibrium lattice constants a_0 (in \AA) together with total μ_{tot} , partial atomic-site resolved μ_{IA} , μ_N and interstitial μ_{int} magnetic moments (in μ_B) as well as total energy difference $\Delta E_{\text{tot}}^{\text{f-p}}$ (Ry) between ferro- and paramagnetic state (in Ry) for RS, WZ and ZB crystal structure.

	$E_{\text{g}}^{\text{up}}(\text{eV})$	$E_{\text{g}}^{\text{dn}}(\text{eV})$	$E_{\text{g}}^{\text{HM}}(\text{eV})$
LiN (RS)	8.05	6.26	0.2
LiN (WZ)	6.56	4.53	0.9
LiN (ZB)	6.55	4.52	1.2
NaN (RS)	5.17	3.12	1.0
NaN (WZ)	4.38	2.20	1.7
NaN (ZB)	4.44	2.37	1.6
KN (RS)	4.54	2.37	2.0
KN (WZ)	3.81	1.72	2.0
KN (ZB)	3.77	1.77	2.0
RbN (RS)	4.22	2.06	2.0
RbN (WZ)	3.48	1.42	2.0
RbN (ZB)	3.45	1.39	2.0

TABLE II: Energy bandgaps for majority up-spin (E_{g}^{up}) and minority down-spin (E_{g}^{dn}) states together with half-metallic bandgaps (E_{g}^{HM}) for three crystal structures.

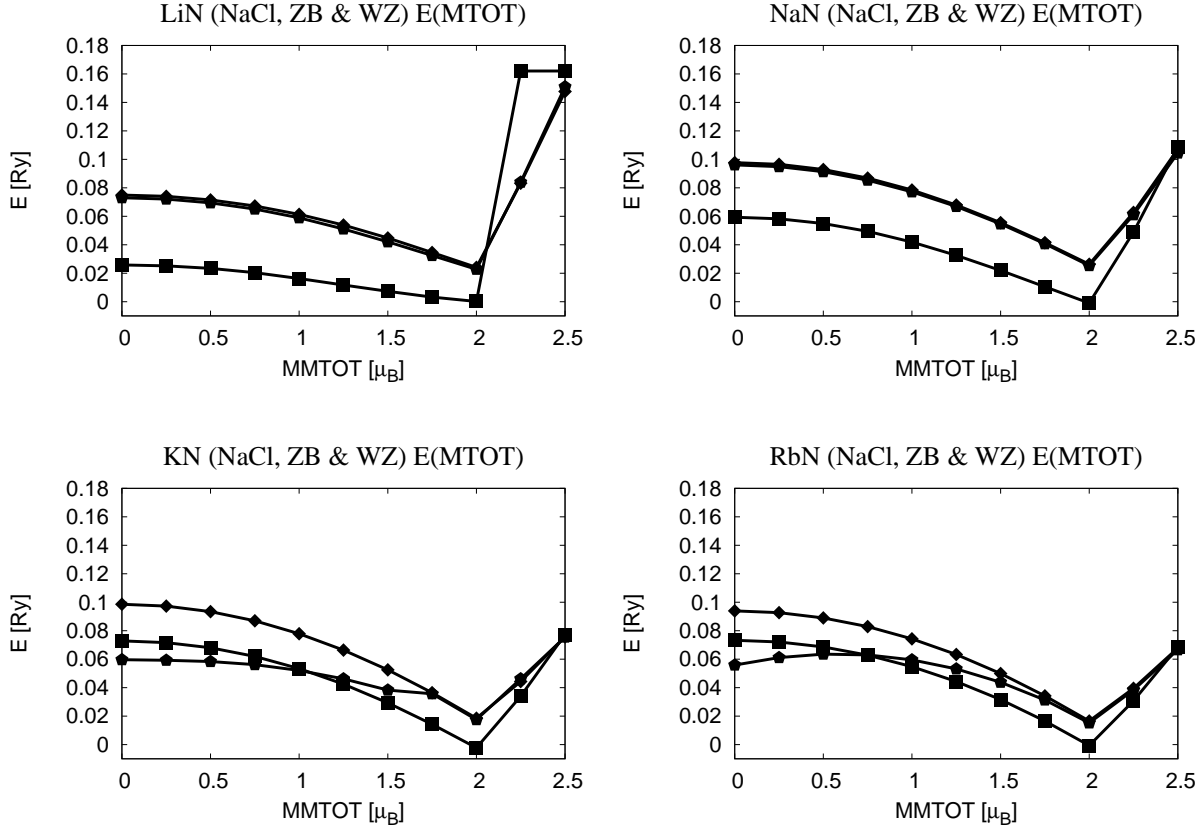


FIG. 2: Total energy E (in Ry), relative to the minimum energy, for LiN, NaN, KN and RbN in equilibrium for three crystal structures (squares – RS, pentagons – WZ, diamonds – ZB) as a function of the assumed net magnetic moment μ_{tot} (in μ_B). Formation of integer magnetic moment $\mu_{\text{tot}} = 2\mu_B$ stabilizes the crystal structure by increasing chemical bonds between I^{A} and N atoms.

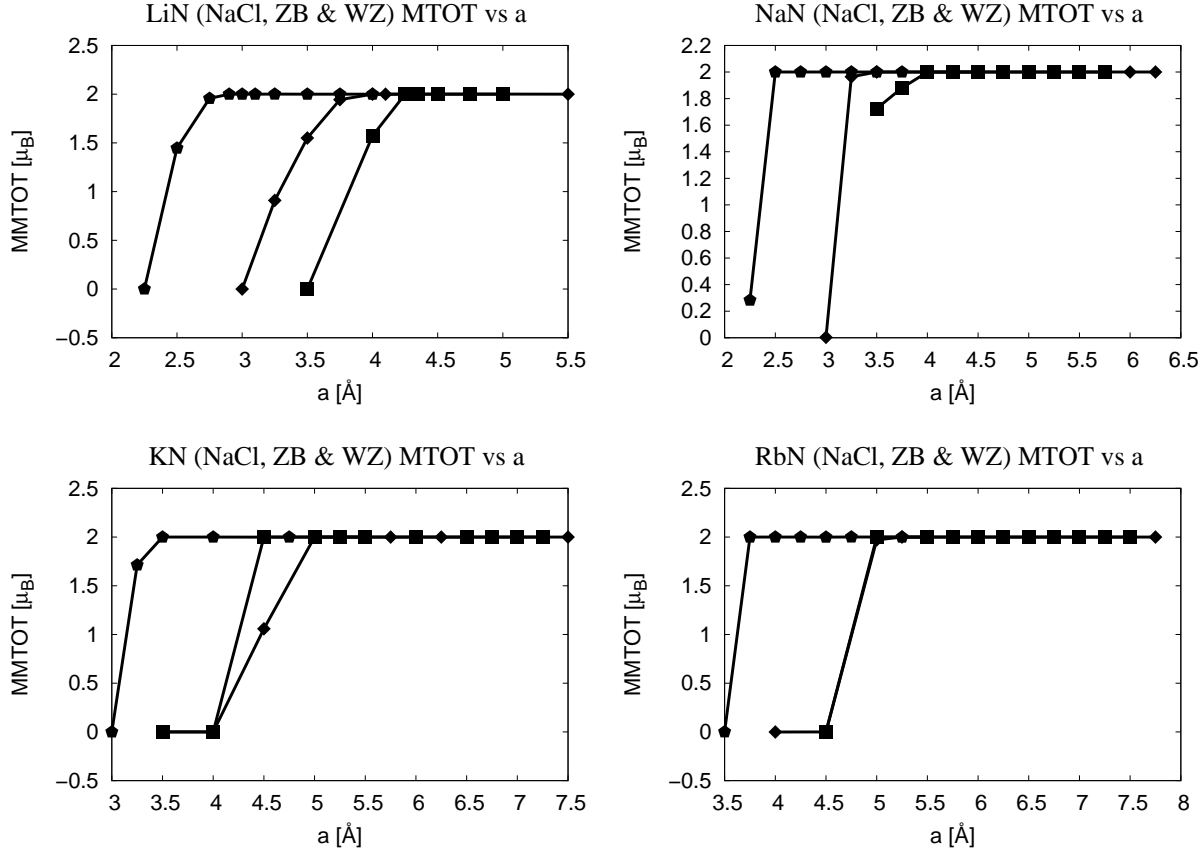


FIG. 3: Magnetic moment μ_{tot} (in μ_B) vs. lattice constant a (in Å) for LiN, NaN, KN and RbN in three crystal structures (squares – RS, pentagons – WZ, diamonds – ZB). The lines are to guide the eye. Critical values of lattice parameter a for compression, below which the total magnetic moment $\mu_{tot} = 2\mu_B$ disappears, can be seen for each compound in three crystal structures. For example, in the case of LiN the critical values of a are 2.75 Å, 3.75 Å and 4.25 Å for WZ, ZB and RS structures, respectively.

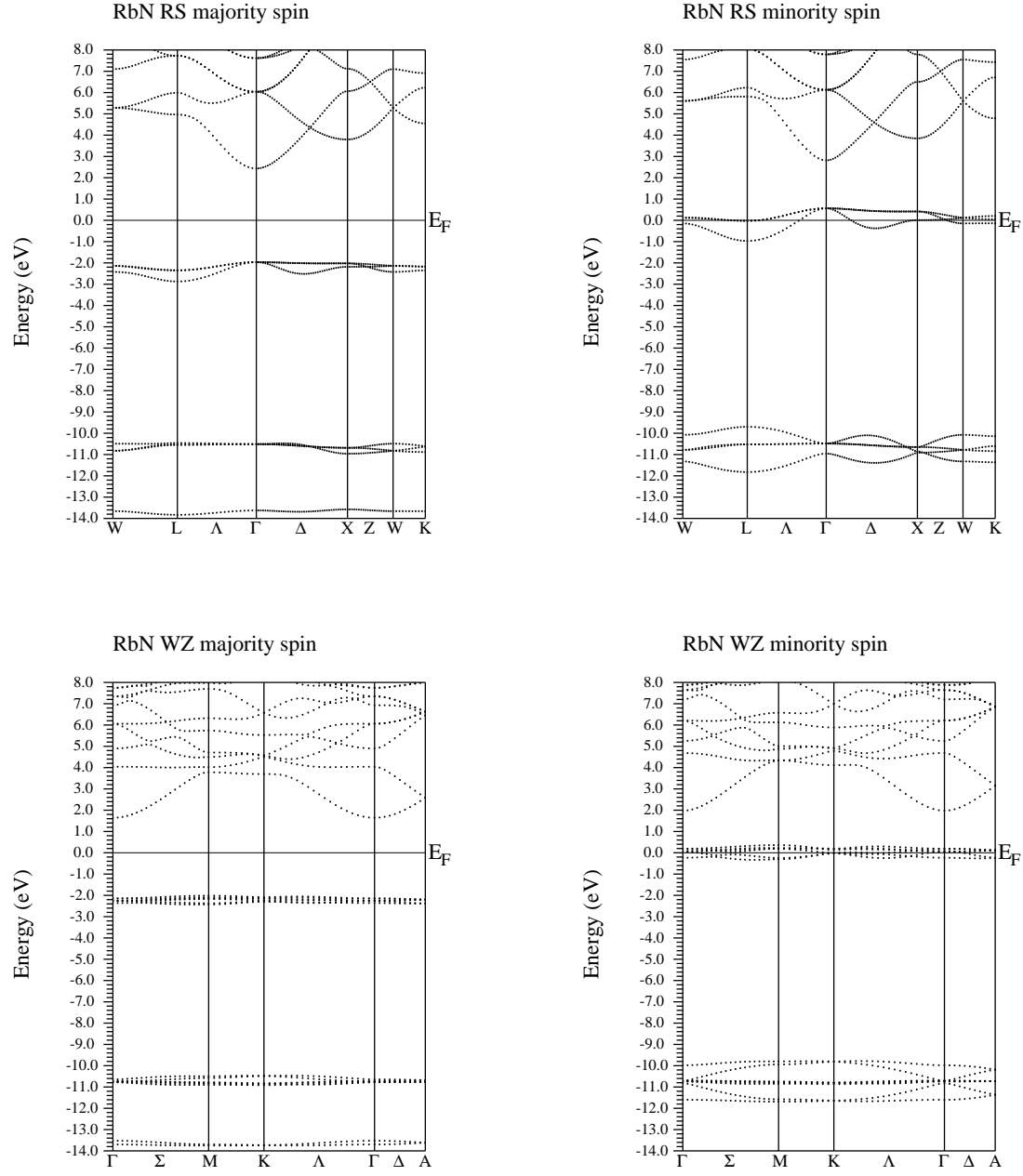


FIG. 4: Spin resolved electron energy bands for RbN in different crystal structures. High symmetry points from the Brillouin zone for two crystal structures are indicated. Highest occupied majority spin (up) subbands, shown in the left-hand-side diagrams, are separated from the Fermi level E_F by half-metallic bandgap $E_g^{\text{HM}} = 2\text{eV}$. The values of bandgaps separating occupied (or partially occupied) and empty states for both majority E_g^{up} and minority (down) E_g^{dn} spin subbands (shown in the right-hand side diagrams) are listed in Table II. Corresponding total and partial DOS are presented in Figure 6.

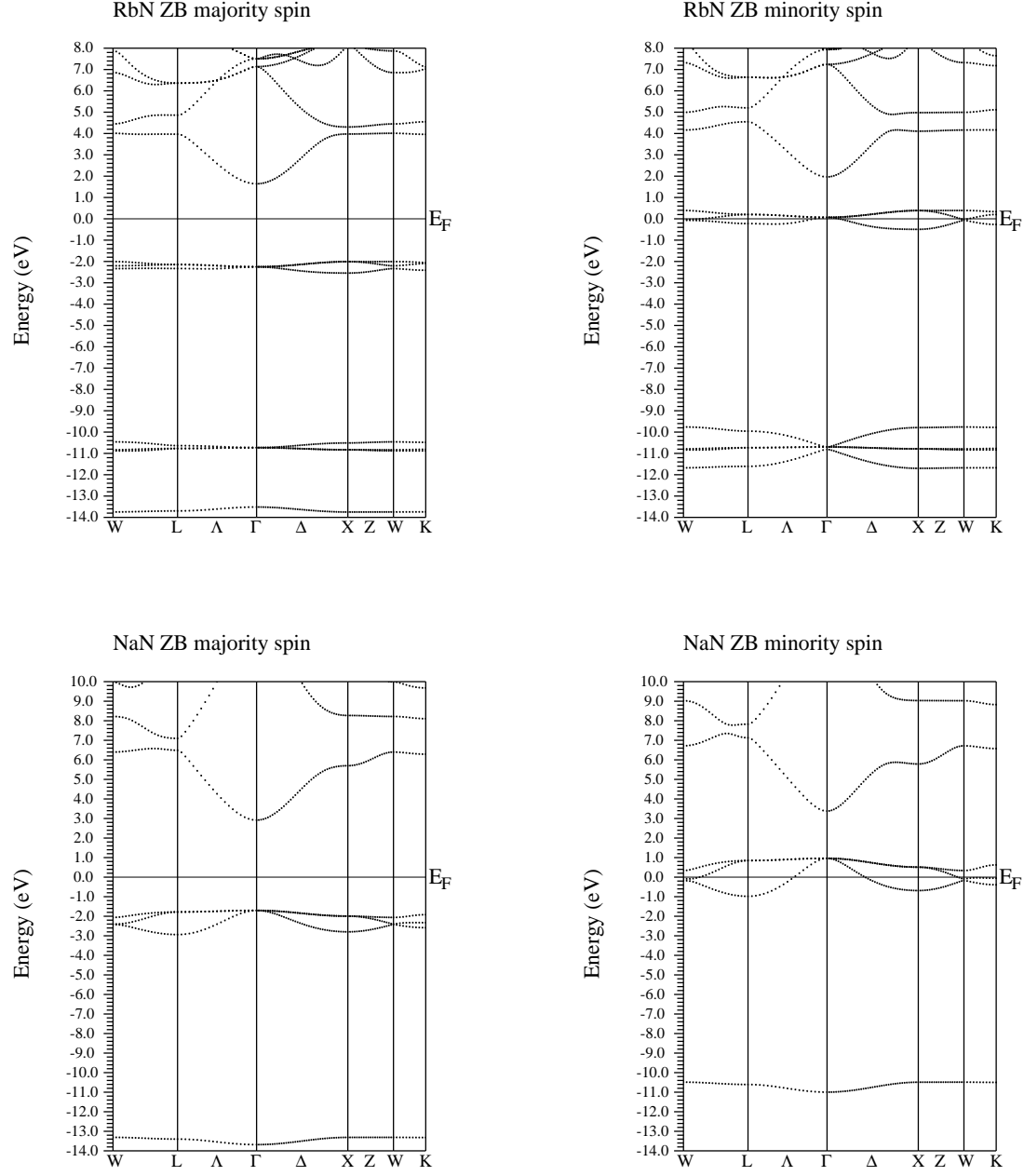


FIG. 5: Spin resolved electron energy bands for RbN and NaN in ZB crystal structure. High symmetry points from the Brillouin zone for ZB crystal structure are indicated. Highest occupied majority spin (up) subbands, shown in the left-hand-side diagrams, are separated from the Fermi level E_F by half-metallic bandgap $E_g^{\text{HM}} = 2\text{eV}$. The values of bandgaps separating occupied (or partially occupied) and empty states for both majority E_g^{up} and minority (down) E_g^{dn} spin subbands (shown in the right-hand side diagrams) are listed in Table II. Corresponding total and partial DOS are presented in Figure 6.

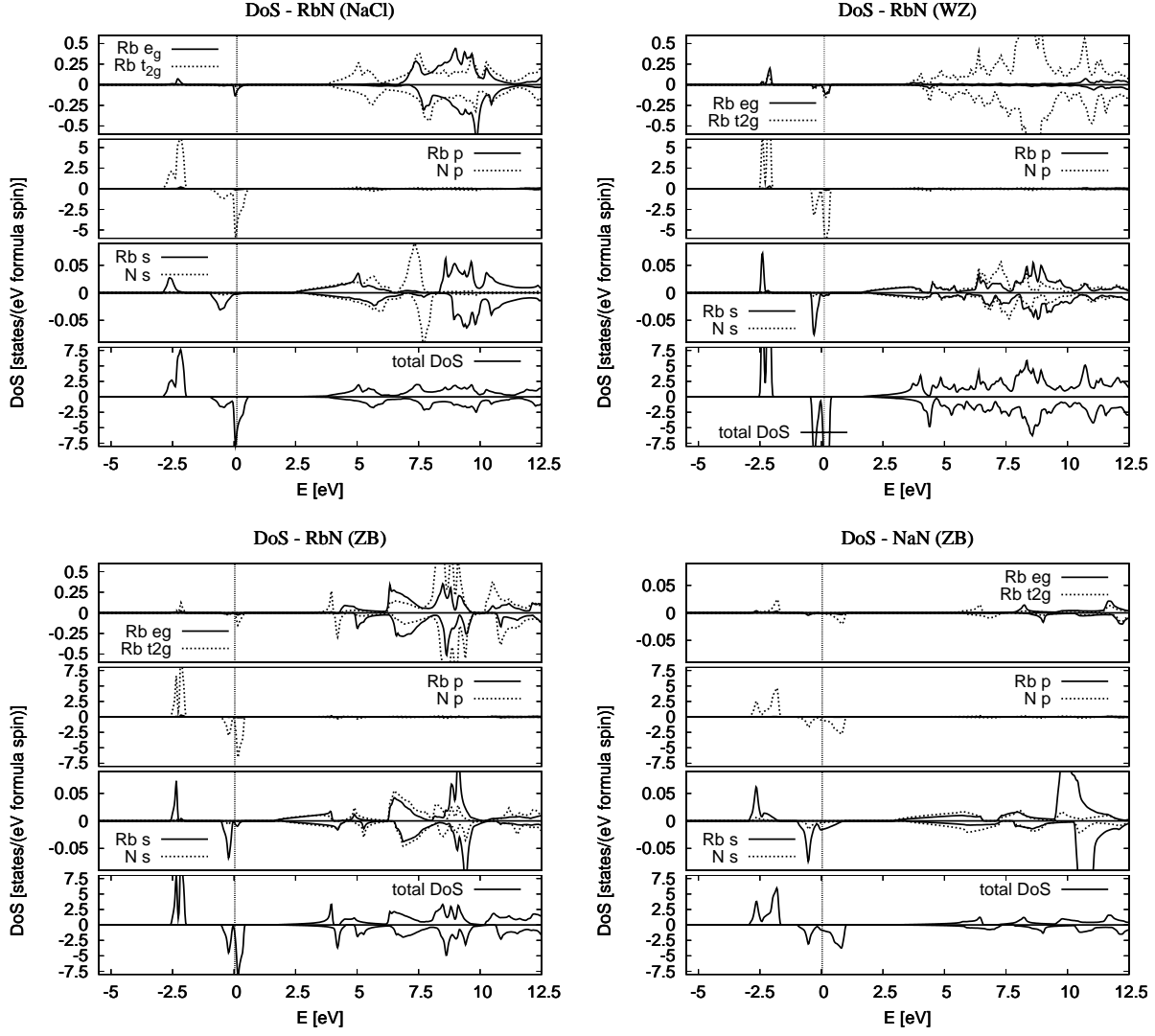


FIG. 6: Total and partial site and symmetry projected DOS for RbN and NaN in different crystalline structures. Angular electron density distribution in the real space for the $d_{x^2-y^2}$ state is in x and y axis, for the state $d_{3z^2-r^2}$ in z axis, what increases the overlap with N p electron states in the RS structure and explains the hybridization between N p and e_g states. On the other hand, angular dependence of t_{2g} states is favored in the ZB structure because of tetrahedral surrounding of neighboring atoms and supports hybridization between N p and t_{2g} states. The hexagonal z axis in WZ structure distinguishes both t_{2g} and e_g Rb states as partners for hybridization with N p states.